ASEN5044 Statistical Estimation of Dynamical Systems
Final Project - Orbit Determination

Joe Miceli
Jose Nido

Spring 2021

Group Member Contributions	
Question 1	Together
Question 2	Together
Question 3	Together
Question 4	Together
Question 5	Together
Final Report	Together

Contents

1 Introduction

Statistical orbit determination is the process of describing the position and velocity of an orbiting spacecraft with high accuracy. The purpose of this project is to implement Kalman filters (KFs) to estimate the states of an orbiting satellite. The scenario will have simulated measurements from 12 ground stations that feed the KFs to perform estimations. We evaluate filter performance examining normalized estimation error square (NEES) and normalized innovation error square (NIS) data. Initial conditions will be defined for the Kalman filter simulations to run, e.g. initial spacecraft state (Cartesian $[x \quad \dot{x} \quad y \quad \dot{y}]^T$) and initial state covariance P. We discuss filter consistency and attempt to tune the filters to meet consistency conditions. Finally, we use the filters to estimate an unknown state and evaluate the results.

1.1 Dynamical System

The continuous time (CT) state of the spacecraft can be defined as 2D position and velocity in an Earth-centered reference frame:

$$X(t) = [x(t) \quad \dot{x}(t) \quad y(t) \quad \dot{y}(t)]^T \tag{1}$$

For brevity, the "t" argument will be omitted and discrete time (DT) variables will be marked with subscripts "k".

The stochastic dynamical system is described by the CT nonlinear (NL) differential equations:

$$\ddot{x}(t) = \frac{-\mu x}{x^2 + y^2}^{\frac{3}{2}} + u_1 + \widetilde{w}_1 \tag{2}$$

$$\ddot{y}(t) = \frac{-\mu y}{x^2 + y^2}^{\frac{3}{2}} + u_2 + \widetilde{w}_2 \tag{3}$$

where $\mu = 398600 \frac{km^3}{s^2}$, u_1 and u_2 are control accelerations, and $\widetilde{w}_1$ and $\widetilde{w}_2$ are disturbances. The dynamics can be written in standard NL state space form (with measurements to be defined later):

$$\dot{X} = \mathcal{F}[X(t), u(t), \widetilde{w}(t)] \tag{4}$$

where

$$\mathcal{F}_1[X(t), u(t), \widetilde{w}(t)] = \dot{x} \tag{5}$$

$$\mathcal{F}_2[X(t), u(t), \widetilde{w}(t)] = \frac{-\mu x}{(x^2 + y^2)^{\frac{3}{2}}} + u_1 + \widetilde{w}_1 \tag{6}$$

$$\mathcal{F}_3[X(t), u(t), \widetilde{w}(t)] = \dot{y} \tag{7}$$

$$\mathcal{F}_4[X(t), u(t), \widetilde{w}(t)] = \frac{-\mu y}{(x^2 + y^2)^{\frac{3}{2}}} + u_2 + \widetilde{w}_2 \tag{8}$$

The nominal state of the spacecraft is assumed to be a circular orbit with radius $r_0 = 6678km$ radius and velocity of $v_0 = r_0\sqrt{\frac{\mu}{r_0^3}}$.

$$X_{nom}(t) = [r_0 cos(nt) \quad -v_0 sin(nt) \quad r_0 sin(nt) \quad v_0 cos(nt)]^T \tag{9}$$

where $n = \frac{2\pi}{period}$ is the mean motion of the spacecraft. The initial state of the spacecraft is then defined as:

$$\begin{aligned} X_{nom}(t_0) &= [x_0 = r_0 \ \dot{x}_0 \ y_0 \ \dot{y}_0 = v_0]^T \\ &= [6678km \ 0km/s \ 0km \ 7.7258km/s]^T \end{aligned} \tag{10}$$

There is also an initial perturbation defined as:

$$\delta X(t_0) = [0 \quad 0.075km/s \quad 0km \quad -0.021km/s]^T \tag{11}$$

that will be used for simulations later. A differential solver, i.e. Matlab's *ode45* can then be used to integrate the dynamics using an initial boundary state which will be defined as:

$$X_0 = X_{nom}(t_0) + \delta X(t_0) \tag{12}$$

1.2 Measurements

The next part of the scenario are the measurements. The measurements are produced by ground stations, whose states are a function of their rotation θ in the X-Y plane . Each ground station i produces measurements $y^i = [\rho \quad \dot{\rho} \quad \phi]^T$ that are derived from the ground site state and satellite state. The i^{th} ground station state is assumed to be known perfectly and is computed by the equations:

$$x_{si}(t) = R_\oplus \cos(\omega_\oplus t + \theta_i(0)) \tag{13}$$

$$\dot{x}_{si}(t) = -\omega_\oplus R_\oplus \sin(\omega_\oplus t + \theta_i(0)) \tag{14}$$

$$y_{si}(t) = R_\oplus \sin(\omega_\oplus t + \theta_i(0)) \tag{15}$$

$$\dot{y}_{si}(t) = -\omega_\oplus R_\oplus \cos(\omega_\oplus t + \theta_i(0)) \tag{16}$$

where $R_\oplus = 6738km$ and $\omega_\oplus = \frac{2\pi}{86400}\frac{rad}{s}$. $\theta_i(t)$ describes the ground stations rotation in the X-Y plane and is related to the ground stations Cartesian position via:

$$\theta_{si}(t) = tan^{-1}(\frac{y_{si}}{x_{si}}) \tag{17}$$

The initial condition $\theta_{si}(0)$ is defined for each ground station as

$$\theta_{si}(0) = (i-1) * \frac{\pi}{6} \tag{18}$$

The true measurements are then defined as follows:

$$Y_{si} = \begin{bmatrix} \rho_{si} \\ \dot{\rho}_{si} \\ \phi_{si} \end{bmatrix} + \tilde{v}_{si} \tag{19}$$

Writing in standard nonlinear state space form:

$$Y_{si} = h_{si}[X, u, \tilde{v}] = \begin{bmatrix} h_{si_1[X,u,\tilde{v}]} \\ h_{si_2[X,u,\tilde{v}]} \\ h_{si_3[X,u,\tilde{v}]} \end{bmatrix} \tag{20}$$

where

$$r_{rel} = [x \quad y]^T - [x_{si} \quad y_{si}]^T \tag{21}$$

$$v_{rel} = [\dot{x} \quad \dot{y}]^T - [\dot{x}_{si} \quad \dot{y}_{si}]^T \tag{22}$$

$$\rho_{si}(t) = ||r_{rel}|| \tag{23}$$

$$\dot{\rho}_{si}(t) = \frac{r_{rel} \cdot v_{rel}}{\sqrt{r_{rel} \cdot r_{rel}}} \tag{24}$$

$$\phi_{si}(t) = tan^{-1}(\frac{y_{si}}{x_{si}}) \tag{25}$$

Due to the geometry of the problem, some ground stations may not be visible to the satellite at a given time (i.e. when the satellite is below the horizon of a ground station, which is optimistic). When this occurs, the ground station is unable to provide a measurement. The visibility can be determined by examining the elevation angle ϕ and θ. That is, ground station i can only provide a measurement if:

$$\phi_{si} \in [-\frac{\pi}{2} + \theta_{si}, \frac{\pi}{2} + \theta_{si}] \tag{26}$$

The visibility for a given ground station was calculated with the following algorithm:

$$\phi_{si}(t) = \text{atan2}((y - y_{si}), (x - x_{si})) \tag{27}$$

$$\alpha = \min[2\pi - (\theta_{si} - \phi_{si}), (\theta_{si} - \phi_{si})] \tag{28}$$

$$\text{if} \quad \alpha_{min} \geqslant \frac{\pi}{2} \Rightarrow \text{no visibility}$$

Now that the scenario has been established, we have all the essentials to apply a Kalman filter. We have an initial state for our satellite, we have the dynamics, and the perturbation. We know the nonlinear equations that define the measurements provided by 12 different ground sites. Utilizing all the scenario elements, a Kalman filter can be applied to do statistical orbit determination.

2 Part I. Deterministic System Analysis

2.1 CT Jacobians and Linearized Model

The nonlinear system can be linearized about the nominal operating point to find the linearized dynamics that describe perturbations to this operating point.

We begin with the assumption that the CT nonlinear model can be written as:

$$\dot{X}(t) = \mathcal{F}[X(t), u(t)] + \Gamma(t)\tilde{w}(t) \tag{29}$$

$$Y(t) = h[X(t), u(t)] + \tilde{v}(t) \tag{30}$$

Using a Taylor Series expansion near the nominal operating point, the CT linearized state space model can be represented as:

$$\delta\dot{X} = \tilde{A}\delta X + \tilde{B}\delta u + \Gamma\tilde{w} \tag{31}$$

$$\delta Y = \tilde{C}\delta X + \tilde{D}\delta u + \tilde{v} \tag{32}$$

Where,

$$\tilde{A} = \frac{\delta\mathcal{F}}{\delta X}, \quad \tilde{B} = \frac{\delta\mathcal{F}}{\delta u}, \quad \tilde{C} = \frac{\delta h}{\delta X}, \quad \tilde{D} = \frac{\delta h}{\delta u} \tag{33}$$

which we will define further later. The perturbation states

$$\delta X = X - X_{nom} \tag{34}$$

$$\delta u = u - u_{nom} = [0\ 0]^T \tag{35}$$

$$\delta Y = Y - H(X_{nom}) \tag{36}$$

To find the CT linearized model parameters, the Jacobians of the nonlinear system parameters must be evaluated at the nominal operating point. The CT linearized system matrix is defined as:

$$\tilde{A} = \frac{\delta\mathcal{F}}{\delta X}\bigg|_{X_{nom},u_{nom}} = \begin{bmatrix} \tilde{A}_{11} & \tilde{A}_{12} & \tilde{A}_{13} & \tilde{A}_{14} \\ \tilde{A}_{21} & \tilde{A}_{22} & \tilde{A}_{23} & \tilde{A}_{24} \\ \tilde{A}_{31} & \tilde{A}_{32} & \tilde{A}_{33} & \tilde{A}_{34} \\ \tilde{A}_{41} & \tilde{A}_{42} & \tilde{A}_{43} & \tilde{A}_{44} \end{bmatrix}\bigg|_{X_{nom},u_{nom}} \tag{37}$$

Where

$$\tilde{A}_{11} = \tilde{A}_{13} = \tilde{A}_{14} = 0$$

$$\tilde{A}_{12} = 1$$

$$\tilde{A}_{21} = \frac{3\mu x^2}{(x^2+y^2)^{\frac{5}{2}}} - \frac{\mu}{(x^2+y^2)^{\frac{3}{2}}}$$

$$\tilde{A}_{22} = \tilde{A}_{24} = 0$$

$$\tilde{A}_{23} = \frac{3\mu xy}{(x^2+y^2)^{\frac{5}{2}}}$$

$$\tilde{A}_{31} = \tilde{A}_{32} = \tilde{A}_{33} = 0$$

$$\tilde{A}_{34} = 1$$

$$\tilde{A}_{41} = \frac{3\mu xy}{(x^2+y^2)^{\frac{5}{2}}}$$

$$\tilde{A}_{42} = \tilde{A}_{44} = 0$$

$$\tilde{A}_{43} = \frac{3\mu y^2}{(x^2+y^2)^{\frac{5}{2}}} - \frac{\mu}{(x^2+y^2)^{\frac{3}{2}}}$$

Note that evaluation at the nominal operating point yields a time-varying dynamics matrix. The CT linearized control matrix is computed in a similar way.

$$\tilde{B} = \frac{\delta \mathcal{F}}{\delta u}\bigg|_{X_{nom},u_{nom}} = \begin{bmatrix} 0 & 0 \\ 1 & 0 \\ 0 & 0 \\ 0 & 1 \end{bmatrix}\Bigg|_{X_{nom},u_{nom}} \tag{38}$$

Note that $\tilde{B}$ is time invariant. Similarly, the CT linearized sensing matrix (also known as measurement sensitivity matrix) can be computed as:

$$\tilde{C}_{si} = \frac{\delta h_{si}}{\delta X}\bigg|_{X_{nom},u_{nom}} = \begin{bmatrix} \tilde{C}_{11} & \tilde{C}_{12} & \tilde{C}_{13} & \tilde{C}_{14} \\ \tilde{C}_{21} & \tilde{C}_{22} & \tilde{C}_{23} & \tilde{C}_{24} \\ \tilde{C}_{31} & \tilde{C}_{32} & \tilde{C}_{33} & \tilde{C}_{34} \end{bmatrix}\Bigg|_{X_{nom},u_{nom}} \tag{39}$$

Where

$$\tilde{C}_{11} = \frac{x - x_{si}}{\sqrt{(x - x_{si})^2 + (y - y_{si})^2}}$$

$$\tilde{C}_{12} = 0$$

$$\tilde{C}_{13} = \frac{y - y_{si}}{\sqrt{(x - x_{si})^2 + (y - y_{si})^2}}$$

$$\tilde{C}_{14} = 0$$

$$\tilde{C}_{21} = \frac{\dot{x} - \dot{x}_{si}}{\sqrt{(x - x_{si})^2 + (y - y_{si})^2}} - \frac{(x - x_{si})^2(\dot{x} - \dot{x}_{si}) + (x - x_{si})(y - y_{si})(\dot{y} - \dot{y}_{si})}{((x - x_{si})^2 + (y - y_{si})^2)^{\frac{3}{2}}}$$

$$\tilde{C}_{22} = \frac{x - x_{si}}{\sqrt{(x - x_{si})^2 + (y - y_{si})^2}}$$

$$\tilde{C}_{23} = \frac{\dot{y} - \dot{y}_{si}}{\sqrt{(x - x_{si})^2 + (y - y_{si})^2}} + \frac{(x - x_{si})(\dot{x} - \dot{x}_{si})(y - y_{si}) + (y - y_{si})^2(\dot{y} - \dot{y}_{si})}{((x - x_{si})^2 + (y - y_{si})^2)^{\frac{3}{2}}}$$

$$\tilde{C}_{24} = \frac{y - y_{si}}{\sqrt{(x - x_{si})^2 + (y - y_{si})^2}}$$

$$\tilde{C}_{31} = -\frac{y - y_{si}}{(x - x_{si})^2 + (y - y_{si})^2}$$

$$\tilde{C}_{32} = 0$$

$$\tilde{C}_{33} = \frac{x - x_{si}}{(x - x_{si})^2 + (y - y_{si})^2}$$

$$\tilde{C}_{34} = 0$$

Note that evaluation along the nominal orbit yields a time-varying matrix. Finally, the process noise to state matrix is interpreted from the original CT NL

dynamics as the time-invariant matrix:

$$\Gamma = \begin{bmatrix} 0 & 0 \\ 1 & 0 \\ 0 & 0 \\ 0 & 1 \end{bmatrix}_{X_{nom}, u_{nom}} \tag{40}$$

We now have the CT Jacobians $\tilde{A}, \tilde{B}, \tilde{C}$, and Γ, needed to linearize the CT system (note that $\tilde{D}$ is [0]). The dimensions of these system matrices are 4x4, 4x2, 3x4, and 4x2 respectively. The dimension of the state X is 4x1 and the dimension of each measurement Y is 3x1.

2.2 Linearized Discrete Time (DT) Model

The Kalman filters implemented for this project will operate in discrete time. Therefore, the CT linearized model previously developed must be discretized. Discretization allows equations 31 and 32 to be written as:

$$\delta X_{k+1} = \tilde{F}_{k|nom[k]} \delta X_k + \tilde{G}_{k|nom[k]} \delta u_k + \tilde{\Omega}_{k|nom[k]} w_k \tag{41}$$

$$\delta Y_{k+1} = \tilde{H}_{k+1|nom[k+1]} \delta X_{k+1} + \tilde{v}_{k+1} \tag{42}$$

For small enough ΔT this discretization can be accomplished via the approximations:

$$\tilde{F}_{k|nom[k]} = e^{\Delta T \tilde{A}_k} \approx I + \Delta T \cdot \tilde{A}\big|_{X_{nom}, u_{nom}, t_k} \tag{43}$$

$$\tilde{G}_{k|nom[k]} = \Delta T \cdot \tilde{B}\big|_{X_{nom}, u_{nom}, t_k} \tag{44}$$

$$\tilde{\Omega}_{k|nom[k]} = \Delta T \cdot \Gamma_{t_k} \tag{45}$$

$$\tilde{H}_{k+1|nom[k+1]} = \tilde{C}\big|_{X_{nom}, u_{nom}, t_{k+1}} \tag{46}$$

For this project, a discretization size of $\Delta T = 10$ seconds will be used. This discretization size is sufficiently small enough to use the above approximations due to the time scales of the problem. The period of the nominal orbit is roughly 5400 secons long so it is expected that the discretized system will be able to reasonably track the nonlinear system for at least one orbit.

In this case, the DT linearized system parameters do change with time. Therefore, conducting an observability analysis would require evaluating an observability matrix at each time step. Similarly, for a controllability analysis of the DT linearized system, the controllability matrix would need to be evaluated at each time step. The observability and controllability of the system can change with time.

2.3 DT Linearized Model Simulation

The linearized DT system is now simulated near the linearization point. The results will then be compared to results of simulating the nonlinear system.

Both simulations will be conducted for 1400 time steps and will be free of process noise, measurement noise, and and control perturbations. The linearized simulation will be initialized with eq. (11). The resulting perturbation at each time step will be added to $X_{nom}(k)$ to get the total state according to eq. (34). The nonlinear simulation will be initialized with eq. (12).

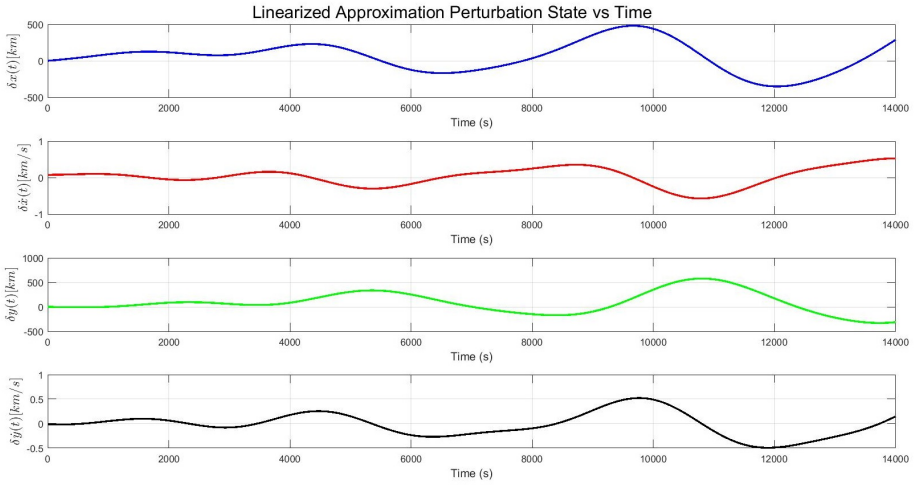

Figure 1: Linearized DT Simulated Perturbation State

For the first 400 seconds of the simulation, the perturbation from the nominal orbit is fairly small. However, figure 1 clearly shows that as time progresses, the perturbation from the nominal state grows dramatically. The perturbation grows to as much as 500km in x-position. In a 300km orbit, this large of difference could mean a collision with the Earth.

The difference between the perturbed total state and nominal state are emphasized in figure 2. These results indicate that,in the linearized model, even a small perturbation from the nominal orbit eventually leads to significant differences in the actual state of the spacecraft. The linearized approximate total state is now compared to the nonlinear true state (obtained using Matlab's *ode45*).

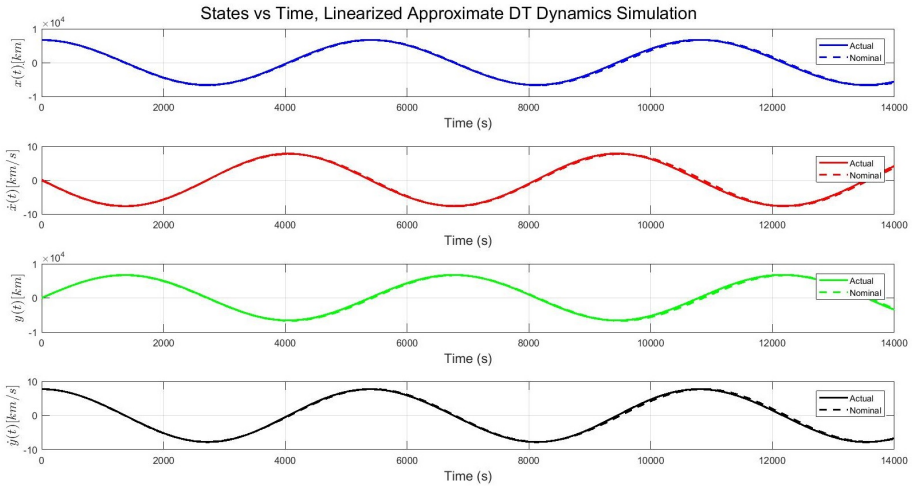

Figure 2: Linearized DT Simulated Total State

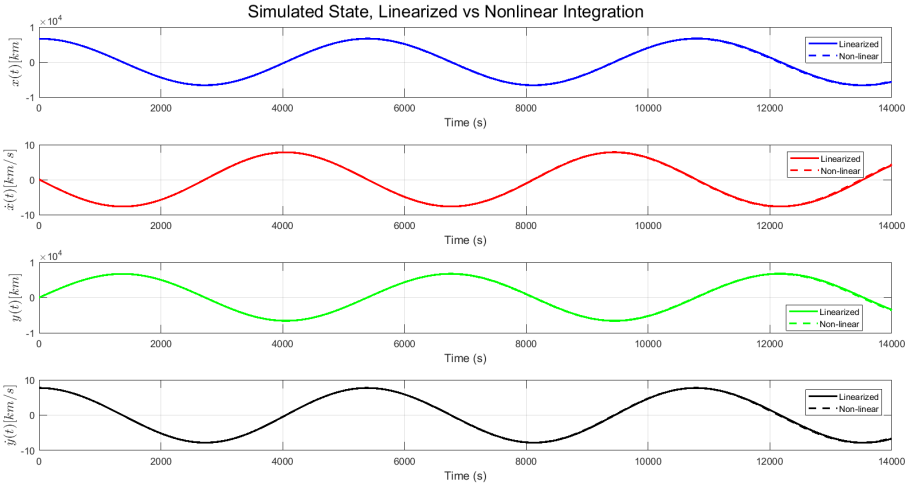

Figure 3: Linearized and Nonlinear DT Simulated State

Figure 3 shows that the linearized approximation of the state does successfully track the true state. As expected, differences between the linearized approximation and the true state grow as time increases. Figures 4 and 5 show that the simulated measurements for the linearized system also closely match the simulated measurements for the nonlinear system. These figures also illustrate the geometry of the problem. Each ground station is only able to provide a measurement for a short period of time. Similarly, it appears that there may be moments where multiple or 0 measurements are available.

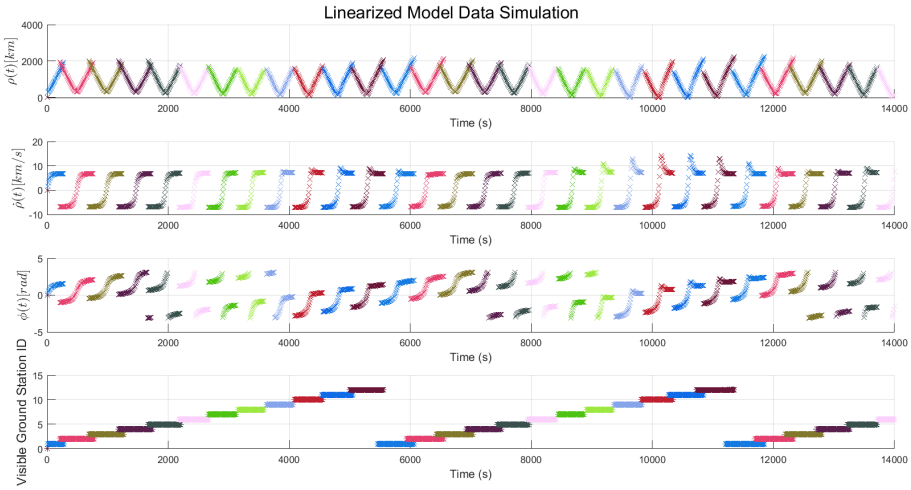

Figure 4: Linearized DT Simulated Measurements

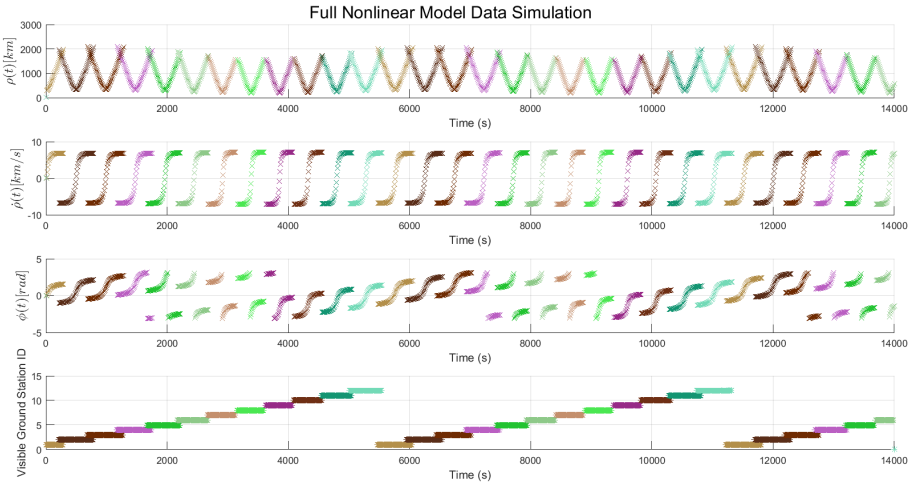

Figure 5: Nonlinear DT Simulated Measurements

3 Part II. Stochastic Nonlinear Filtering

In this section two different nonlinear Kalman filters will be presented. Their algorithms will be discussed. Many Monte-Carlo simulations will be conducted to evaluate filter consistency. A Kalman filter is considered "consistent" if the following conditions hold:

1. Unbiased estimation error: $\mathbb{E}[e_{x,k}] = 0$ for all k
2. Efficiency: true state errors match filter covariance, $\mathbb{E}[e_{x,k}e_{x,k}^T] = P_k^+$
3. KF measurement innovations are white Gaussian processes:

$$e_{y,k} \sim \mathcal{N}(0, S_k) \tag{47}$$

$$\mathbb{E}[e_{y,k}e_{y,k}^T] = S_k \tag{48}$$

Where

$$e_{y,k} = y_k - \hat{y}_k \tag{49}$$

$$S_k = HP_k^- H^T + R \tag{50}$$

The filters will be tuned to attempt to satisfy these consistency conditions. Finally, the overall performance of each filter will be discussed.

Simulations of each Kalman filter will include the generation of simulated measurement data and truth data in what is referred to as Monte-Carlo Truth Model Testing (TMT). 50 simulations will be conducted and the truth data for each simulation will be used to run and evaluate the Kalman filter. Simulated measurements are needed to actually run each filter and evaluate measurement innovations. Simulated truth states are needed to evaluate filter efficiency and error biases. The simulated truth data will be generated with simulated process noise w_k and the simulated measurement data will be generated with simulated measurement noise v_k.

$$w_k \sim \mathcal{N}(0, Q_{true}) \quad v_k \sim \mathcal{N}(0, R_{true}) \tag{51}$$

where Q_{true} is the process noise covariance and R_{true} is the measurement noise covariance provided in the assignment:

$$Q_{true} = \begin{bmatrix} 1 \times 10^{-10} & 0 \\ 0 & 1 \times 10^{-10} \end{bmatrix} \quad R_{true} = \begin{bmatrix} 0.01 & 0 & 0 \\ 0 & 1 & 0 \\ 0 & 0 & 0.01 \end{bmatrix} \tag{52}$$

3.1 General KF Algorithm

Kalman filters follow the same general steps to obtain a state estimate:

1. Propagate/Pure Prediction: propagate the state by integrating the state dynamics from time k to $k+1$ and propagate the covariance with the state transition matrix (or the linearized approximation of it) and process noise covariance.

2. Measurement Update: process measurements (if applicable) and use them to update the predicted estimate. Note that we can iterate through the measurement sets at time k from each observatory facility.

3.2 NEES and NIS Statistics

To evaluate consistency of a filter, two statistical strategies can be used. Namely, the Normalized Estimation Error Squared (NEES) Chi-square and Normalized Innovation Squared (NIS) Chi-square tests. NEES and NIS are two statistics defined as

$$NEES = \epsilon_{x,k} = e_{x,k}^T (P_k^+)^{-1} e_{x,k} \tag{53}$$

$$NIS = \epsilon_{y,k} = e_{y,k}^T (S_k)^{-1} e_{y,k} \tag{54}$$

It can be shown that if

$$\epsilon_{x,k} \sim \mathcal{X}_n^2 \qquad \epsilon_{y,k} \sim \mathcal{X}_p^2 \tag{55}$$

where

$$\mathbb{E}[\epsilon_{x,k}] = n \qquad \mathbb{E}[\epsilon_{y,k}] = p \tag{56}$$

$$var(\epsilon_{x,k}) = 2n \qquad var(\epsilon_{y,k}) = 2p \tag{57}$$

then the consistency conditions hold.

TMT can be utilized to estimate the expectation of NEES and NIS statistics. If $\bar{\epsilon}_{x,k} \approx n$ and $\bar{\epsilon}_{y,k} \approx p$ then the consistency conditions are likely to hold. If N Monte-Carlo simulations are performed, the expectation of the NEES and NIS statistics at time step k can be calculated via:

$$\bar{\epsilon}_{x,k} = \sum_{i=1}^{N} \epsilon_{x,k} \tag{58}$$

$$\bar{\epsilon}_{y,k} = \sum_{i=1}^{N} \epsilon_{y,k} \tag{59}$$

3.3 Linearized Kalman Filter

A linearized Kalman Filter (LKF) is a nonlinear Kalman filtering approach that propagates an estimate of a system's perturbed state using linearized versions of a system's nonlinear dynamics. The total state can then be computed by adding it to a nominal state. The nominal state can be determined "offline" (i.e. before running the filter) by solving the ODE:

$$\dot{X}^*(t) = \mathcal{F}[X^*(t), u^*(t)] \tag{60}$$

The general algorithm for the LKF was modified slightly to account for possible periods of "no measurement." In these cases, the measurement-update

step is skipped and the state estimate and covariance is determined through pure prediction only. In cases where multiple measurements were available, the first received measurement was used. The algorithm is summarized below:

initialize $X_0^+, P_0^+, \delta u_0 = u_0 - u_0^*$

for $k = 1 : nSteps$

$$\delta \hat{X}_{k+1}^- = \tilde{F}_k \delta \hat{X}_k^+ + \tilde{G}_k \delta u_k \tag{61}$$

$$P_{k+1}^- = \tilde{F}_k P_k^+ \tilde{F}_k^T + \tilde{\Omega}_k Q_k \tilde{\Omega}_k^T \tag{62}$$

$$\delta u_{k+1} = u_{k+1} - u_{k+1}^* \tag{63}$$

if measurement available

$$\tilde{H}_{k+1} = \left.\frac{\partial h}{\partial X}\right|_{X_{k+1}^-} \tag{64}$$

$$K_{k+1} = P_{k+1}^- \tilde{H}_{k+1}^T (\tilde{H}_{k+1} P_{k+1}^- \tilde{H}_{k+1}^T + R_{k+1})^{-1} \tag{65}$$

$$\delta Y_{k+1} = Y_{k+1} - h(X_{k+1}^*) \tag{66}$$

$$\delta \hat{X}_{k+1}^+ = \delta \hat{X}_{k+1}^- + K(\delta Y_{k+1} - \tilde{H}_{k+1} \delta \hat{X}_{k+1}^-) \tag{67}$$

$$P_{k+1}^+ = (I - K_{k+1} \tilde{H}_{k+1}) P_{k+1}^- \tag{68}$$

else

$$\delta \hat{X}_{k+1}^+ = \delta \hat{X}_{k+1}^- \tag{69}$$

$$P_{k+1}^+ = P_{k+1}^- \tag{70}$$

update total state estimate

$$\hat{X}_{k+1}^+ = X_k^* + 1 + \delta \hat{X}_{k+1}^+ \tag{71}$$

Where $\tilde{F}_k, \tilde{G}_k, \tilde{\Omega}_k$ and $\tilde{H}_{k+1}$ are the Jacboians evaluated at X^*, u^* defined earlier. Note that Q_k cannot be explicitly solved for like in linear Kalman filters. In this case, Q_k will have to be "tuned" to ensure the filter meets the consistency conditions. The LKF was initialized with an initial perturbation and covariance of

$$\delta X_0 = [0 \quad 0 \quad 0 \quad 0]^T$$

$$P_0^+ = \begin{bmatrix} 0.1 & 0 & 0 & 0 \\ 0 & 0.001 & 0 & 0 \\ 0 & 0 & 0.1 & 0 \\ 0 & 0 & 0 & 0.001 \end{bmatrix} \tag{72}$$

Physically, this means that the filter believes the spacecraft is starting in the nominal orbit and is fairly confident in this prediction. Recall that the diagonal elements of P represent variance of each element of the state. Standard deviations of 0.316 km in position and 0.0316 km/s in velocity are reasonable for a satellite in orbit.

First, the LKF is examined using $Q_k = Q_{true}$. The results from this simulation are shown below. While the state estimate appears accurate, the esti-

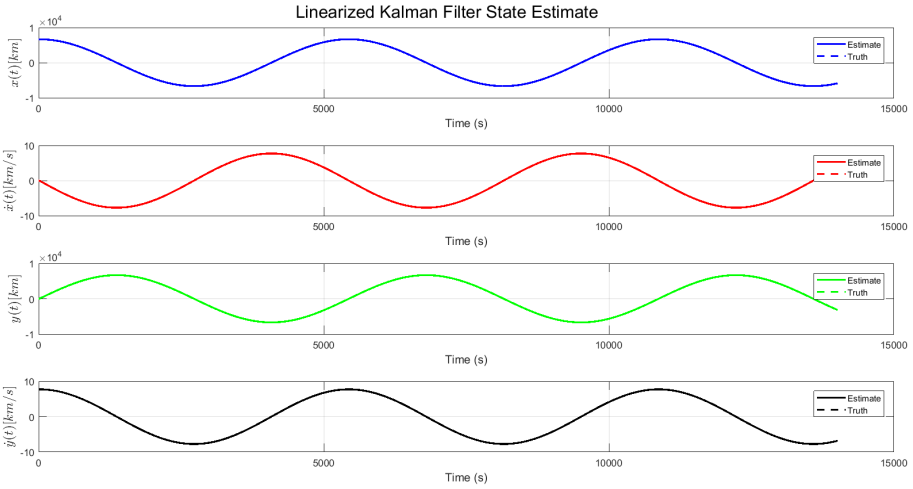

Figure 6: Typical LKF State Estimate Using Q_{true} as Approximate Process Noise Intensity Covariance

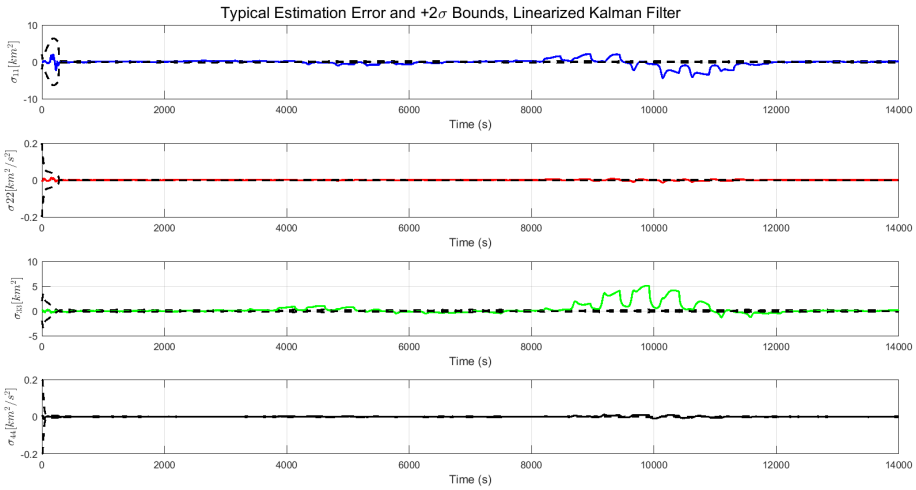

Figure 7: Typical LKF State Estimation Error and Covariance Using Q_{true} as Approximate Process Noise Intensity Covariance

mation error and NEES and NIS statistics reveal that the filter is performing rather poorly. A position error of up to 5km is unacceptable for most spacecraft applications. This is not surprising in that Q_{true} represents the process noise

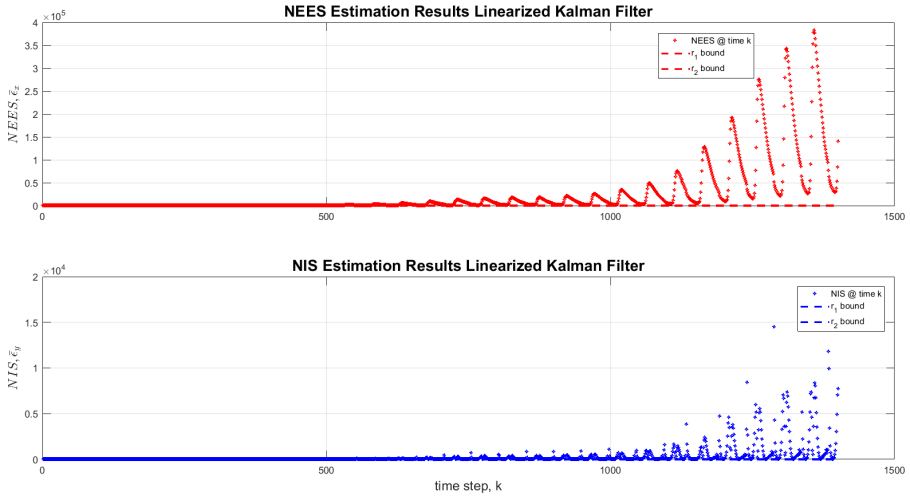

Figure 8: LKF NEES and NIS Statistics Using Q_{true} as Approximate Process Noise Intensity Covariance

covariance of the nonlinear system rather than the linearized system.

3.3.1 LKF NEES and NIS Statistics

To evaluate the consistency of the LKF, the NEES and NIS statistics can be used. Becuase we are evaluating the mean over a finite number of simulations, we will use a significance level, $\alpha = 0.01$, to evaluate the NEES and NIS hypothesis tests. In other words, the tests will investigate if the NEES and NIS points are within the interval in which 99% of NEES and NIS values *should* be. Using the definition of the NEES and NIS statistics and examining figure 8, it is clear that Q_k is currently too low. The LKF is very "smug". It believes its estimates are much more accurate than they actually are. The value of Q_k was iteratively tuned and the NEES and NIS results as well as the estimation error were examined after every change.

After dozens of trials, the values of Q_k and R_k that produced the best results were

$$Q_k = \begin{bmatrix} 2 \times 10^{-10} & 5 \times 10^{-11} \\ 5 \times 10^{11} & 2 \times 10^{-10} \end{bmatrix} \quad R_k = R_{true} \tag{73}$$

Figures 9, 10, and 11 summarize the results of implementing this value of Q_k in the LKF.

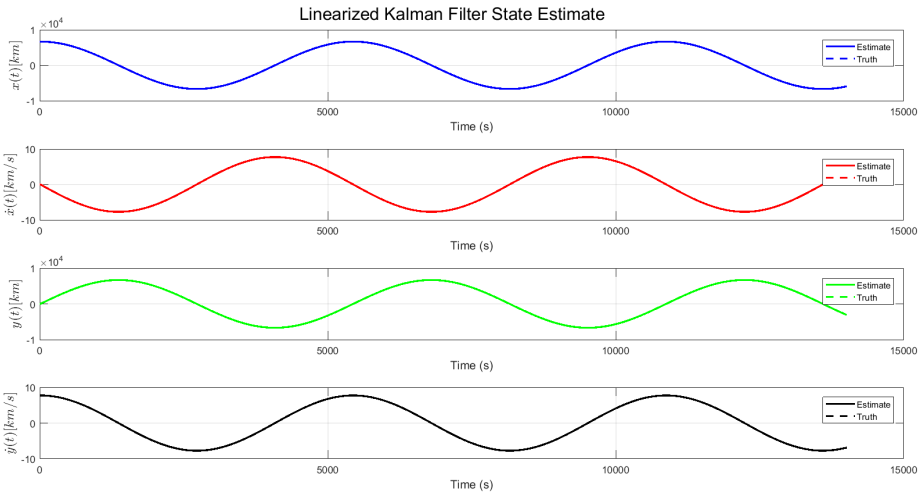

Figure 9: Typical LKF State Estimate Using Updated Q_k as Approximate Process Noise Intensity Covariance

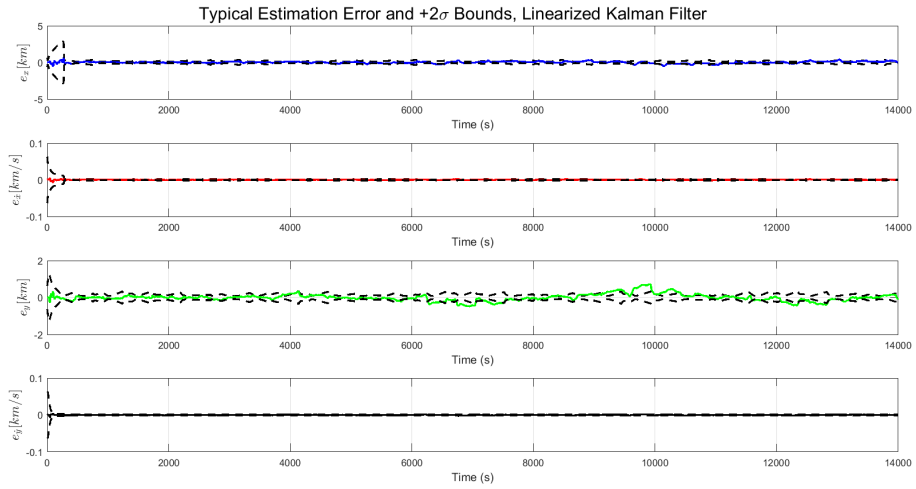

Figure 10: Typical LKF State Estimation Error and Covariance Using Updated Q_k as Approximate Process Noise Intensity Covariance

The results of these simulations indicate that the filter is still smug. The LKF is able to remain consistent for nearly 300 time steps (3000 seconds) but, as time increases, the filter becomes more overconfident in its estimates. Increasing Q_k should have resulted in decreasing NEES and NIS values. However, we found that both increasing and decreasing Q_k from this value resulted in fewer NEES and NIS values near the significance interval as well as increased

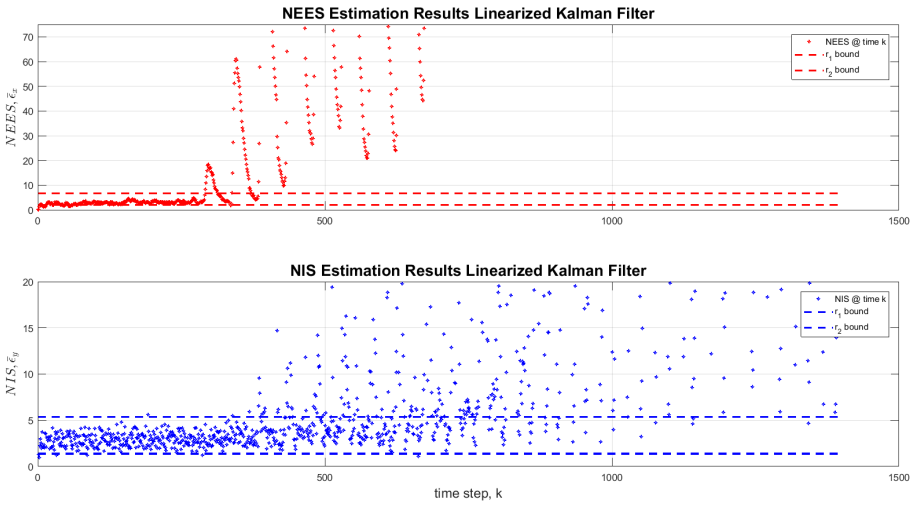

Figure 11: LKF NEES and NIS Statistics Using Updated Q_k as Approximate Process Noise Intensity Covariance

estimation error. Though the LKF does not meet consistency conditions for the entire simulation, this agrees with the behavior observed in the simulation of the linearized dynamics. As time increases, the discrepancies between the linearized and nonlinear dynamics grow.

3.4 Extended Kalman Filter

An extended Kalman filter (EKF) is another nonlinear Kalman filtering approach. It operates in a similar way to the LKF in that it linearizes the nonlinear system dynamics $\mathcal{F}$ to construct a portion of its estimate. However, two key differences are that the EKF linearizes the nonlinear system about the current estimated state (rather than a nominal state) and also utilizes those nonlinear dynamics when constructing its updated estimate. This allows the EKF to directly estimate a total state rather than a perturbation. Similarly to the LKF, the general algorithm for the EKF was modified to account for periods of "no measurement" or multiple measurements. The same strategy employed in the LKF will be used in the EKF to mitigate these situations. The EKF algorithm is summarized below:

initialize X_0^+, P_0^+, u_0

for $k = 1 : nSteps$

$$\hat{x}_{k+1}^- = f(\hat{x}_k^+, u_k, w_k = 0) \tag{74}$$

$$\tilde{F}_k = I + \Delta T \cdot \tilde{A}\big|_{\hat{x}_k^+, u_k, t_k} \tag{75}$$

$$P_{k+1}^- = \tilde{F}_k P_k^+ \tilde{F}_k^T + \tilde{\Omega}_k Q_k \tilde{\Omega}_k^T \tag{76}$$

if measurement available

$$\tilde{H}_{k+1} = \frac{\delta h}{\delta X}_{\hat{x}_{k+1}^-} \tag{77}$$

$$\hat{y}_{k+1}^- = h[\hat{x}_{k+1}^-, v_{k+1} = 0] \tag{78}$$

$$\tilde{e}_{y_{k+1}} = y_{k+1} - \hat{y}_{k+1}^- \tag{79}$$

where y_{k+1} is the received measurement

$$\tilde{K}_{k+1} = P_{k+1}^- \tilde{H}_{k+1}^T (\tilde{H}_{k+1} P_{k+1}^- \tilde{H}_{k+1}^T + R_{k+1})^{-1} \tag{80}$$

$$\hat{x}_{k+1}^+ = \hat{x}_{k+1}^- + K_{k+1} \tilde{e}_{y_{k+1}} \tag{81}$$

$$P_{k+1}^+ = (I - K_{k+1} \tilde{H}_{k+1}) P_{k+1}^- \tag{82}$$

else

$$\hat{X}_{k+1}^+ = \hat{X}_{k+1}^- \tag{83}$$

$$P_{k+1}^+ = P_{k+1}^- \tag{84}$$

Again, the approximate process noise covariance, Q_k will have to be "tuned" to ensure the filter meets the consistency conditions. The EKF was initialized with the following initial state and covariance:

$$\hat{X}_0^+ = [6678\ 0\ 0\ 7.7258]^T \quad P_0^+ = \begin{bmatrix} 1 & 0 & 0 & 0 \\ 0 & 0.01 & 0 & 0 \\ 0 & 0 & 1 & 0 \\ 0 & 0 & 0 & 0.01 \end{bmatrix} \tag{85}$$

Physically, this means the filter believes that the spacecraft is initially in the nominal orbit (and is fairly confident about this prediction). Truth data for these simulations however, will be generated using an initial state that is perturbed from the nominal orbit (defined in eq. 12).

Again, the EKF is first examined using $Q_k = Q_{true}$. The results from this simulation are shown in figures 12, 13, and 14. Clearly, the EKF is able to produce more accurate estimates than the LKF when using Q_{true} as an estimate of the process noise intensity covariance. This is because the EKF is integrating the same nonlinear dynamics that were used to generate the truth data as opposed to taking linear approximations of these dynamics. Therefore, Q_{true} is an accurate estimate of the true process noise intensity covariance. The EKF meets consistency conditions already. No tuning is needed. That is

$$Q_k = Q_{true} \quad R_k = R_{true} \tag{86}$$

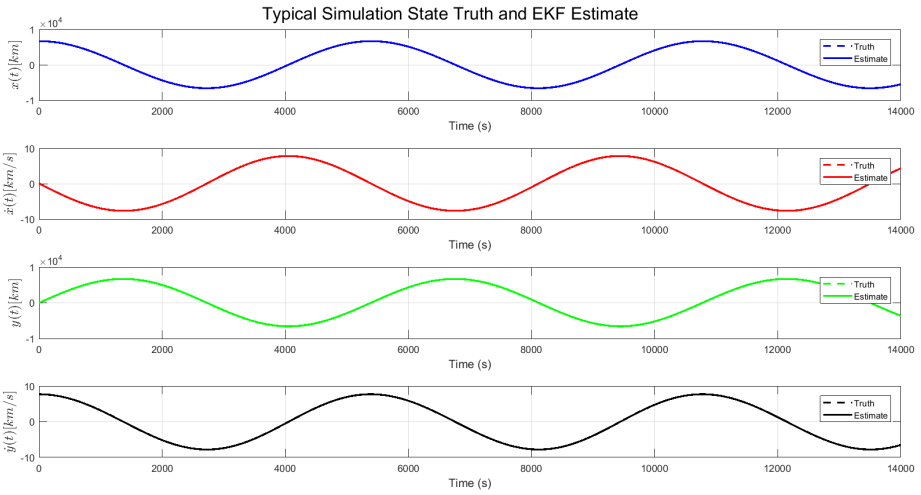

Figure 12: Typical EKF State Estimate Using Q_{true} as Approximate Process Noise

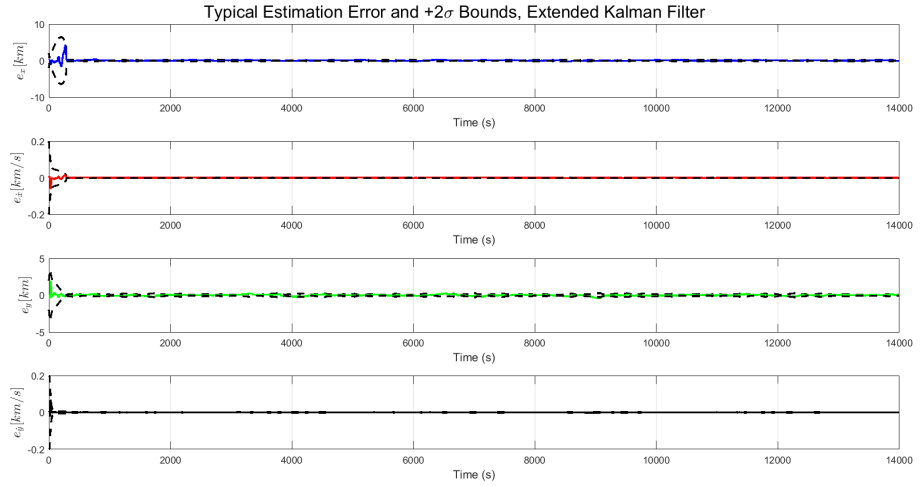

Figure 13: Typical EKF State Estimation Error and Covariance Using Q_{true} as Approximate Process Noise

3.4.1 EKF NEES and NIS Statistics

As shown in figure 14, the EKF is consistent. Nearly all of the expectations for NEES and NIS statistics fall within the chosen significance interval for the entire simulation. Q_k was adjusted to verify that Q_{true} actually is the best estimate for process noise intensity covariance. Increasing Q_k above Q_{true} made the filter more "pessimistic," it lowered the NEES and NIS values and made the

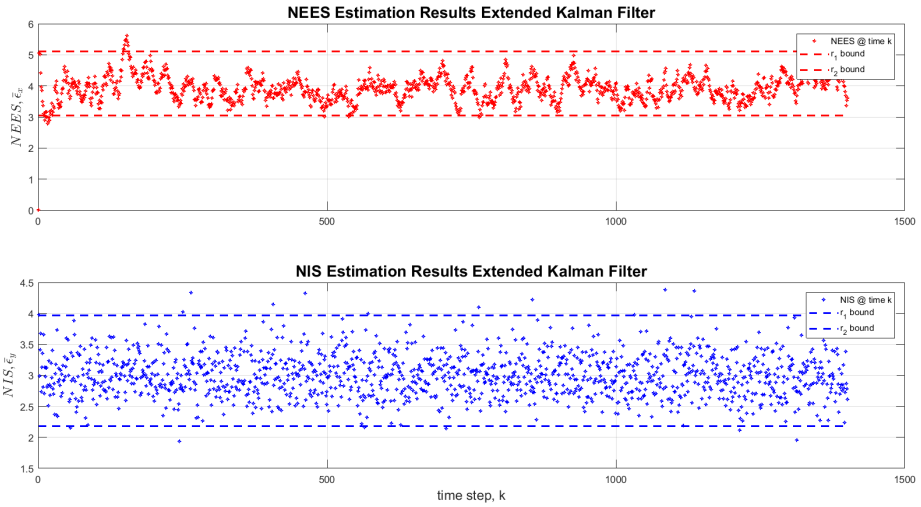

Figure 14: EKF NEES and NIS Statistics Using Q_{true} as Approximate Process Noise

filter think it was performing worse than it actually was. On the otherhand, decreasing Q_k made the filter more "smug," it raised NEES and NIS values and made the filter overconfident in its estimates. Figures 15 and 16 show these affects. It should be noted that, in practice, Q_{true} would be unknown and the filter would have needed to be tuned.

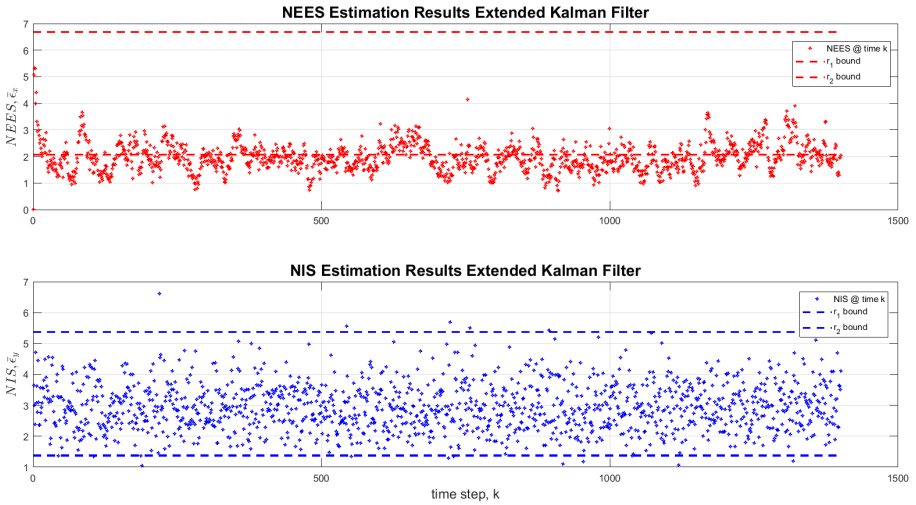

Figure 15: EKF NEES and NIS Statistics Using $Q_k = 5 * Q_{true}$

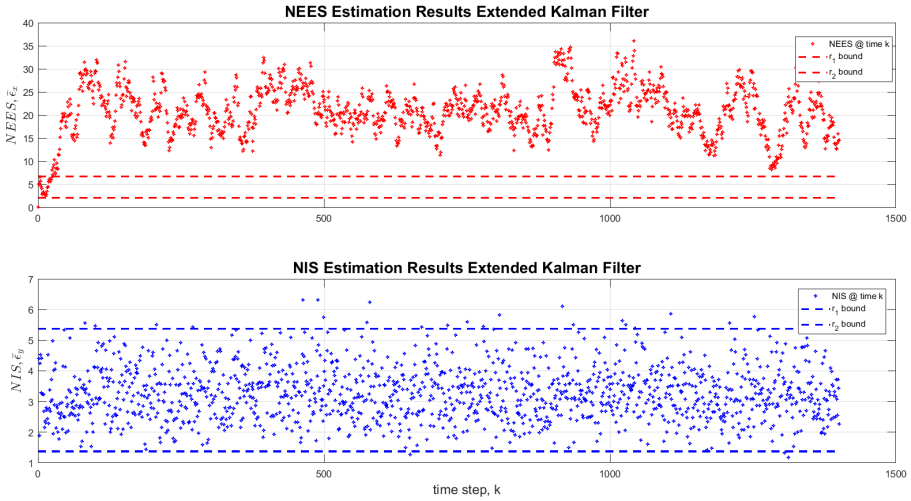

Figure 16: EKF NEES and NIS Statistics Using $Q_k = 0.1 * Q_{true}$

3.5 Estimation of an Unknown State

Up to this point, the "true" state of the spacecraft has been generated via TMT. The LKF and EKF will now be used to estimate an unknown orbit using provided measurements. The performance of each filter will be evaluated.

The filters will use the "tuned" values of Q_k and R_k determined earlier. The LKF will use the same initial condition defined in eq. 72. The EKF will use the same initial condition defined in eq. 85. While the initial condition is not known in this application, it is assumed that the spacecraft is beginning near the nominal circular orbit. As before, if multiple observations are provided at a given time step, the first measurement received is used. If no measurements are provided at a given time step, the measurement update step is skipped, the estimate is obtained from pure prediction only. The results of the filter estimates are shown in figures 17 and 18.

3.5.1 Comparing the LKF and the EKF

Though the true state of the spacecraft is unknown in this application, figures 17 and 18 clearly show the EKF provides a better estimate than the LKF. The LKF's noisy estimate is unlikely to be physically possible. To add, the EKF's estimate provides superior confidence in its estimate; which is clear through its lower 2σ bounds for each element of its estimate.

3.5.2 Analysis of EKF Measurement Innovations

For analysis purposes, the measurement innovations (defined by eq. 79) were plotted along with their associated 2σ bounds. Recall the definition of innova-

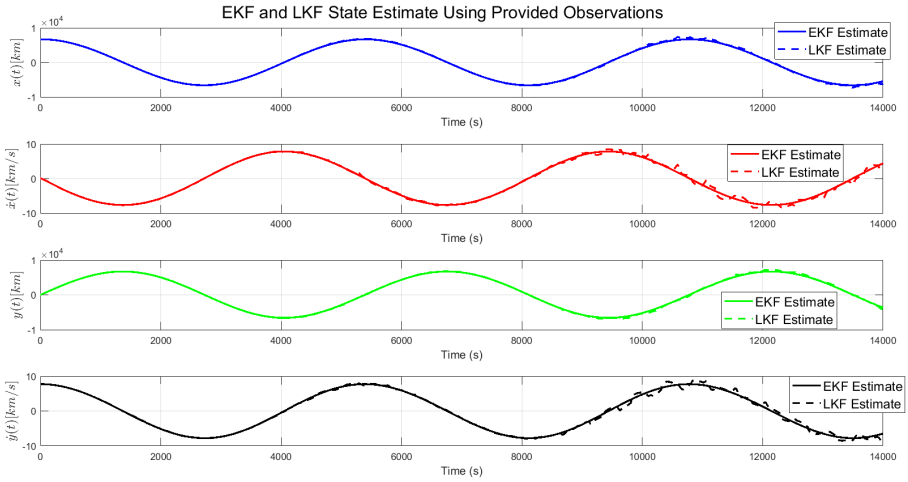

Figure 17: EKF and LKF Estimates of Unknown State

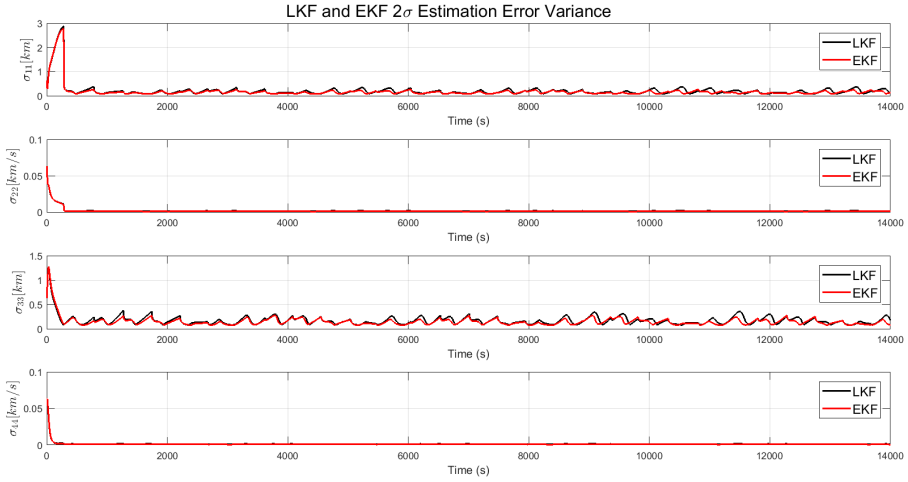

Figure 18: EKF and LKF Estimation Error $+2\sigma$ Bounds

tion covariance defined as:

$$S_{k+1} = \tilde{H}_{k+1} P_k^- \tilde{H}_{k+1}^T + R_{k+1} \tag{87}$$

Due to the fact that measurements are not always available, the measurement innovation does not exist every time step. The results are shown in figure 19 and are surprisingly noisy. Innovations this noisy likely do not have a significant impact on the actual state estimation because of the size of the Kalman gain, $\tilde{K}_{k+1}$. The low Q_k relative to R_k implies that the filter has high confidence

in the model and places more trust in its time estimate update than in its measurement update.

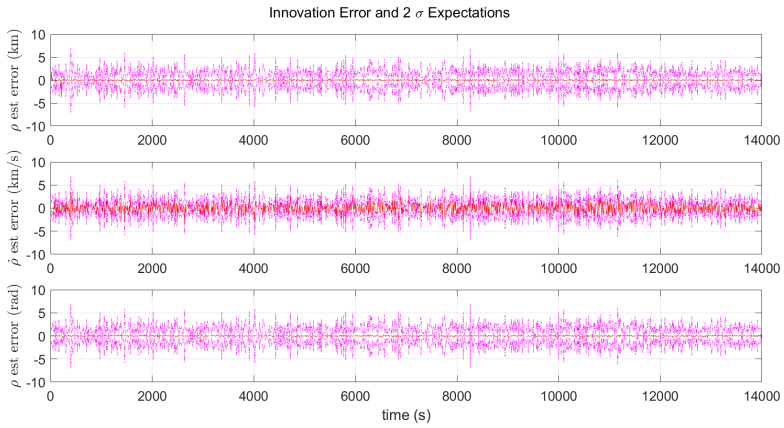

Figure 19: EKF Innovation and 2σ Bounds

4 Conclusion

The goal of this project was to perform orbit determination of a satellite given range, range rate, and elevation measurements from multiple observatories using a linearized kalman filter and an extended kalman filter. We derived the discrete time linearized dynamical system from the continuous time non-linear system. We summarized the algorithms for both the LKF and EKF. We then implemented the filters in Matlab and evaluated them. Truth Model Testing was used to evaluate NEES and NIS statistics and identify if the filters met conditions for consistency. Our results show that the LKF introduces discrepancies between the linearized and non-linear dynamics that become significant after some time. This implies the LKF is good for relatively shorter periods of time and a smaller time step. The EKF showed much better results because, instead of linearizing the dynamics, non-linear integration of the dynamics is used for the prediction. Note that both the LKF and the EKF must be tuned to approximate the process noise covariance of the system. Both the LKF and EKF are sensitive to the initialization parameters, such as initial covariance, state, measurement variance, and process noise covariance. There are several initialization methods but we used engineering judgement to identify a reasonable initial state and covariance. Upon setting the initial conditions to for the filters, the simulations were executed. Unlike the LKF diverging after some time, the EKF was able to confidently predict the satellite state after processing the given measurements. In conclusion we have implemented and tested LKFs and EKFs and used these filters to process given measurements for statistical orbit determination of a satellite.

5 Appendix

5.1 Advanced Questions

5.1.1 An Estimation Haiku

Propagate a state
Receive a measurement and
Update prediction!

5.2 Additional Part I Plots

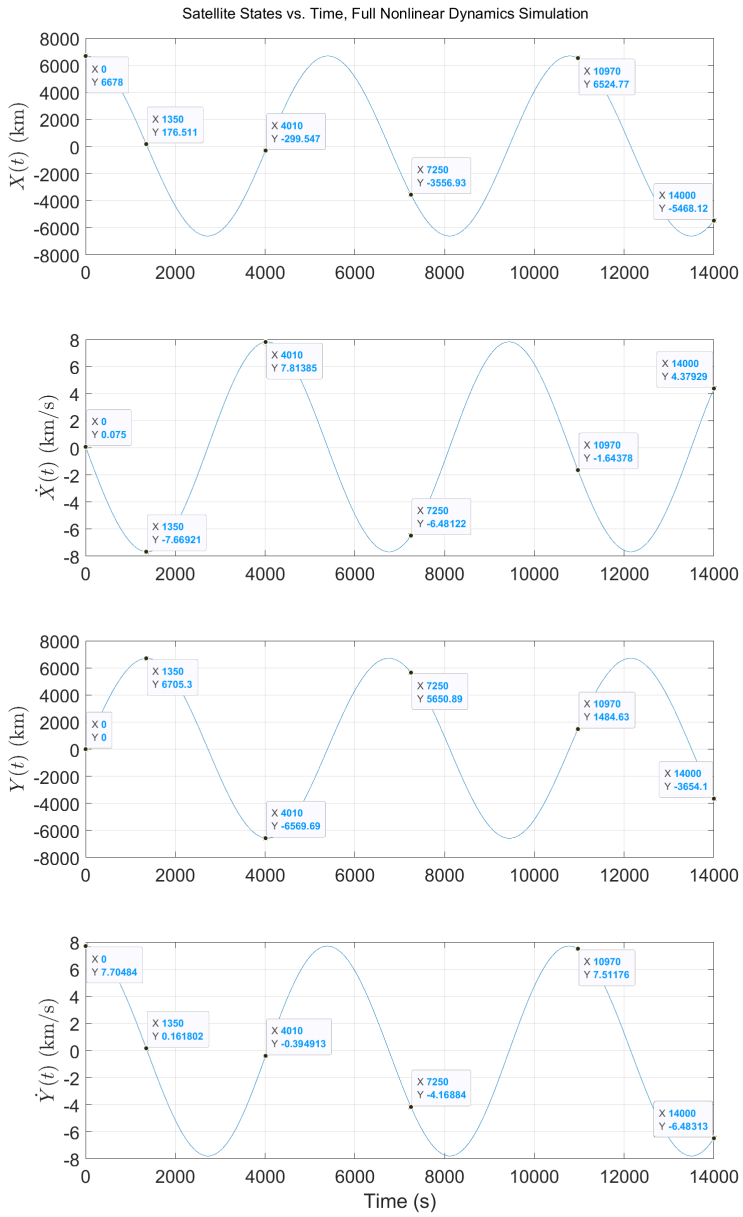

Figure 20: Initial nominal state + perturbation propagated using non-linear 2body acceleration dynamics. Compare to "OrbitDeterm_Part1SolnSketch.pdf" see also `ORBIT_DETERMINATION_PROGRAM.m`

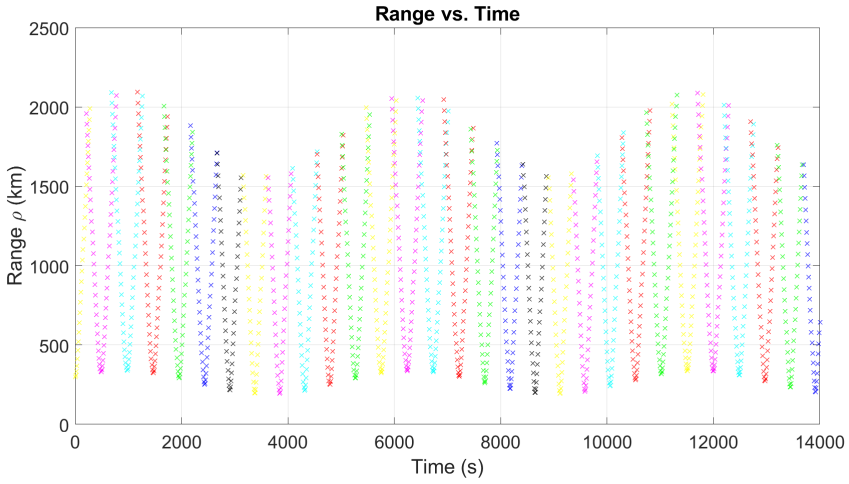

Figure 21: Range measurements from all ground sites, when accessible. Compare to "OrbitDeterm_Part1SolnSketch.pdf" see also `ORBIT_DETERMINATION_PROGRAM.m`

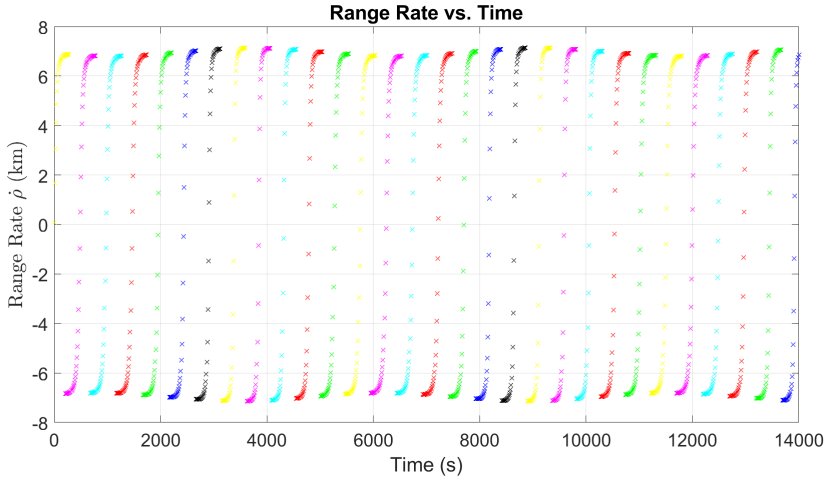

Figure 22: Range rate measurements from all ground sites, when accessible. Compare to "OrbitDeterm_Part1SolnSketch.pdf" see also `ORBIT_DETERMINATION_PROGRAM.m`

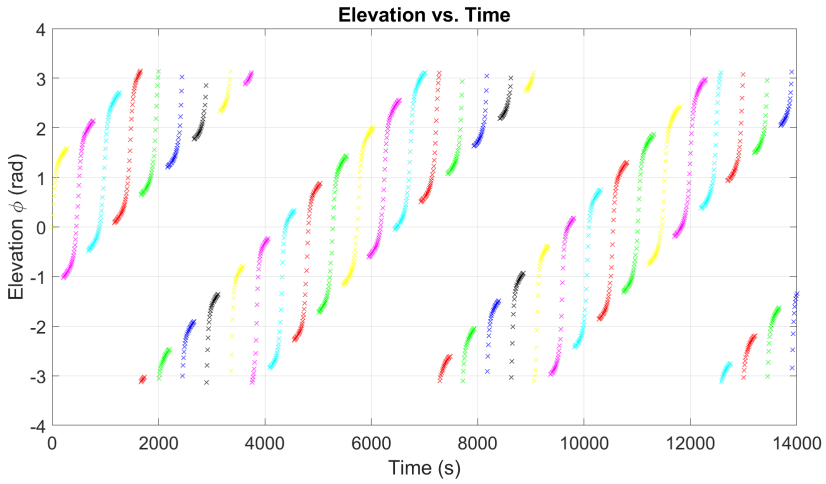

Figure 23: Elevation measurements from all ground sites, when accessible. Compare to "OrbitDeterm_Part1SolnSketch.pdf" see also `ORBIT_DETERMINATION_PROGRAM.m`

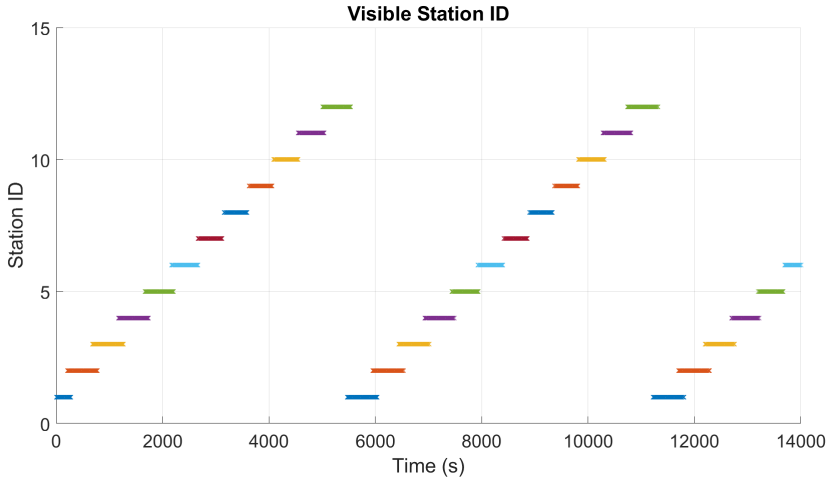

Figure 24: Station ID, when accessible. Compare to "OrbitDeterm_Part1SolnSketch.pdf" see also `ORBIT_DETERMINATION_PROGRAM.m`

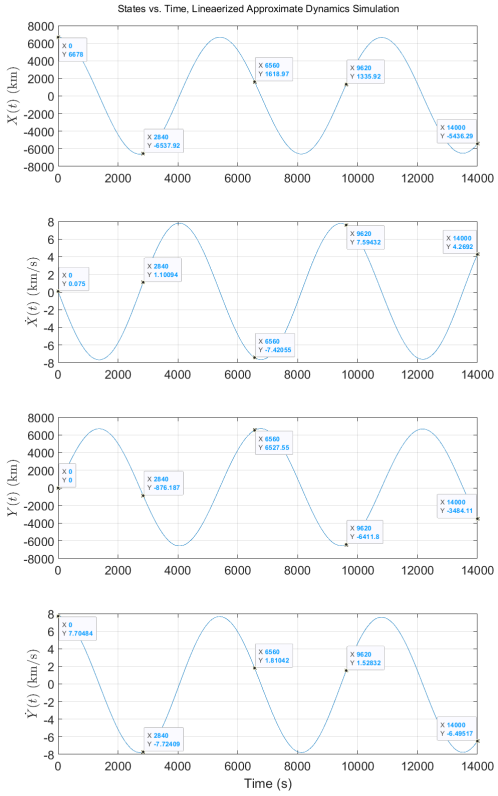

Figure 25: Nominal solution + linear approx. propagation of the perturbation. Compare to "OrbitDeterm_Part1SolnSketch.pdf" note that there is a bit of a deviation from solution sketch as the sim time continues. See also `ORBIT_DETERMINATION_PROGRAM.m`

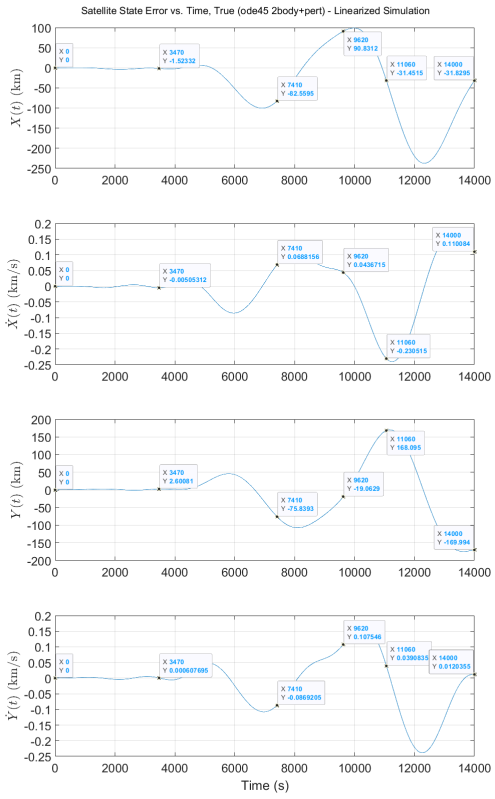

Figure 26: State Error vs Time: True (ode45 `Xnom+pert`$_x 0 Nominal - linear approx. The two solutions are in family. See also$ `ORBIT_DETERMINATION_PROGRAM.m`